Advanced Physics Lab
Zeeman Effect

Vladislav Bushmakin, Samuel Tovey

June 23, 2019

Abstract

The Longitudinal and transverse emission lines in the Zeeman effect are observed. The Paschen-Back effect is induced in the sample such that a bohr magneton value of $9.204 \cdot 10^{-24}$ can be derived. Furthermore, a polarization experiment is performed allowing for the transition to π lines to be observed.

1 Introduction

The Zeeman effect is a broad term encompassing effects related to spectral lines exposed to magnetic fields wherein a splitting of their energy levels will be observed. The Zeeman effect is a useful tool in characterising energy levels of atoms as well understanding quantum theory. In this experiment, the spectral line splitting of Helium $3^3D - 2^3P, \lambda = 568.6nm$ is observed under different magnetic field strengths in order to observe the Zeeman and Paschen-Back effect[1].

2 Theory

2.1 Multiplet systems

In atomic physics, a multiplet systems is an atom with more than one valence electron. This results in the total angular momentum of the atom being comprised of multiple components and requires additional treatment when coupling. In practice this coupling is done in several ways depending on the system being studied. Russel-Saunders or LS coupling is employed when the interaction between the spin and the orbital angular momentum of the individual electrons in the systems is smaller than the interaction between the spin and orbital angular momentum of the other electrons. In this coupling, the individual spins add together to make a spin vector **S**, as do the orbital angular momentum terms add linearly to form a single angular momentum vector **S**. These vectors can then be added to form the total angular momentum of the system **j**. This combination can occur in any linear combination of the spins and angular momentum of the individual electrons, leading to the following rule. For a system with total momentum's **L** and **S**, the system can exist in any total momentum value from $|L + S|$ to $|L - S|$ in integer steps, so long as it is allowed by the Pauli Principle. This will be expanded in section 2.5 as an analysis of the Helium atom is performed. For much heavier atom there is a scheme known as jj coupling wherein the interaction between spin and orbital angular momentum in an individual atom is greater or comparable to that between different electrons. This is only possible in much heavier atoms and is not relevant to the experiment and thus, will not be discussed here[2].

2.2 Zeeman Effect

The Zeeman effect as mention in the Introduction is a term used to describe the splitting of spectral lines in the presence of a magnetic field. There are two types of Zeeman effect that need addressing, normal and anomalous. The difference comes down to the system being in a S=0 state or not and how the terms couple as a result of this. However, to develop a full understanding it is important to study the mechanism with quantum mechanics[2].

2.2.1 Normal Zeeman Effect

To begin the analysis with quantum mechanics the magnetic field is written as a gauge transformation using the vector potential A and electric field strength F.

$$\mathbf{B} = \nabla \mathbf{A} \tag{1}$$

$$\mathbf{F} = -\nabla V - \frac{d\mathbf{A}}{dt} \tag{2}$$

Using this formalism, it is possible to write down the Hamiltonian of the system so that it can be analysed.

$$\mathscr{H} = -\frac{\hbar^2}{2m_0}\nabla^2 + \frac{e}{m_0}\mathbf{A}\mathbf{p} + \frac{e\hbar}{2m_0 i}\nabla \cdot \mathbf{A} + \frac{e^2\mathbf{A}^2}{2m_0} + V \tag{3}$$

The magnetic field is chosen to be along the z axes, thus, the vector potential may be written.

$$A_x = -\frac{B_z}{2}y, A_y = \frac{B_z}{2}x, A_z = 0 \tag{4}$$

This is applied to equation 3 to produce the following.

$$[\frac{\hbar^2}{2m_0}\nabla^2 + B_z\frac{e}{2m_0}\frac{\hbar}{i}(x\frac{\partial}{\partial y} - y\frac{\partial}{\partial x}) + \frac{e^2B_z^2}{8m_0}(x^2+y^2) + V(r)]\psi = E\psi \tag{5}$$

Assuming then a spherically symmetric potential as well as a standard solution for the wavefunction.

$$\frac{\hbar}{i}(x\frac{\partial}{\partial y} - y\frac{\partial}{\partial x}) = \hat{l}_z = \frac{\hbar}{i}\frac{\partial}{\partial\phi} \tag{6}$$

$$\Psi(r) = R_{n,l}(\mathbf{r})e^{im\phi}P_l^m(\cos\theta) \tag{7}$$

A final energy can be derived.

$$E = E_n^0 + B_z\frac{e\hbar}{2m_0}m, -l \leq m \leq l \tag{8}$$

which, as one can see, is the standard energy of the system shift by some amount dependant on the strength of the applied magnetic field and the atomic number m. When this is coupled with the selection rules $\delta m = 0, \pm 1$ this leads to the normal Zeeman effect. Furthermore, equation 8 introduces the important Bohr magneton, defined as $\mu_B = \frac{e\hbar}{2m_0}$.

2.2.2 Anomalous Zeeman Effect

The anomalous Zeeman effect is very similar to the normal however it incorporates spin and thus, requires spin-orbit coupling as well as coupling between the spin and the magnetic field. This means the Schrödiner equation is written as follows[2].

$$[\frac{1}{2m_0}(\frac{\hbar}{i}\nabla + e\mathbf{A})^2 + V + \frac{e}{m_0}\hat{\mathbf{s}}\cdot\mathbf{B}]\psi = i\hbar\frac{\partial\Psi}{\partial t} \tag{9}$$

and the interaction energy can be written.

$$\frac{\mu_0 Z}{4\pi r^3}(\mu_{\hat{orbit}}\cdot\mu_{\hat{spin}}) \tag{10}$$

This leads to the time independent Schrödinger equation being written.

$$[-\frac{\hbar^2}{2m_0}\nabla^2 - \frac{Ze^2}{4\pi\epsilon_0 r} + \frac{e}{2m_0}B\hat{l}_z + \frac{e}{m_0}\hat{s}_z B + \frac{Ze^2\mu_0}{8\pi m_0^2 r^3}(\hat{\mathbf{l}}\cdot\hat{\mathbf{s}})]\psi = E\psi \tag{11}$$

It is best now to relabel this equation in terms of the corrections, this leads to the following.

$$[\mathscr{H}_0 + W_{magn} + W_{spin-orbit}]\psi = E\psi \tag{12}$$

By re-writing these equations in terms of their operators one can finally derive the form of the energy correction.

$$\delta E_{j,l,m_j} = \frac{e\hbar}{2m_0}Bg\cdot m_j \tag{13}$$

where g is the famous lande-g factor which can be written as.

$$g = 1 + \frac{j(j+1) - l(l+1) + s(s+1)}{2j(j+1)} \tag{14}$$

Thus, one can see that there is a difference in the energy splitting when the spin of the system is involved[2].

2.3 Paschen-Back Effect

In the above cases, it has always been assumed that the magnetic field is weak. This is to say that the interaction between he spin and orbital angular momentum of the individual electrons is greater than the coupling to the field. It is then interesting to study what may occur when the field becomes strong enough that this is no longer true, this regime leads to the so called Paschen-Back effect[2]. In this regime, the magnetic field dissolves the fine structure constant such that l and s are uncoupled and precess around the $\mathbf{B}_0$ field. This leads to a magnetic energy for the system as well as a new energy correction in the spectral lines.

$$V_{m_s,m_l} = (m_l + 2m_s)\mu_B \mathbf{B}_0 \tag{15}$$

$$\delta E = (\delta m_l + 2\delta m_s)\mu_B \mathbf{B}_0 \tag{16}$$

This transition also has selection rules, namely $\delta m_l = 0, \pm 1$ for π and σ transitions as well as $\delta m_s = 0$. This effect leads to a splitting of spectral lines and can be used to better characterize and atomic species[2]. These selection rules will be discussed in section 2.4.

2.4 Selection Rules and Polarization

As has been previously stated, transitions between Zeeman states only takes place according to a set of selection rules, namely $\delta L = 0, \pm 1$, $\delta S = 01$, $\delta J = 0, \pm 1$, $\delta m_j = 0, \pm 1$. Furthermore, we must add that a transition of any $\delta m = \pm 1$ are labelled σ transitions and are induced by circularly polarized light, conversely, a transition of $\delta m = 0$ is denoted a π transition and is performed induced by plane polarized light. These conditions come about due to consequences of Fermi's golden rule and the Hamiltonian of light matter interaction. Specifically, upon solving for the dipole moment in an electron-photon system, one finds that only a number of energetic transitions are possible, thus producing the selection rules[3].

2.5 Visible He Spectrum

Helium is a useful atom to study as it is the simplest of the many-electron atoms being of only 2 electrons. When the Helium atom is excited, one of its electrons will remain it its ground state whilst the other is excited into a higher state. As light interaction cannot induce a spin flip, Helium exists in one of two states, a singlet, or a triplet. These refer to the total spin of the system and thus, angular momentum. In the singlet state, Helium has no fine structure and a total spin of 0, that is to say, the spins of the two electrons are anti-parallel, these systems are referred to as parahelium. In its other state, the two electron spins do not cancel each other out and the system has a net spin angular momentum of 1. In this system referred to as orthohelium, there is indeed a fine structure and magnetic moment which results in interaction in magnetic fields. The spectrum of Helium is best understood diagrammatically.

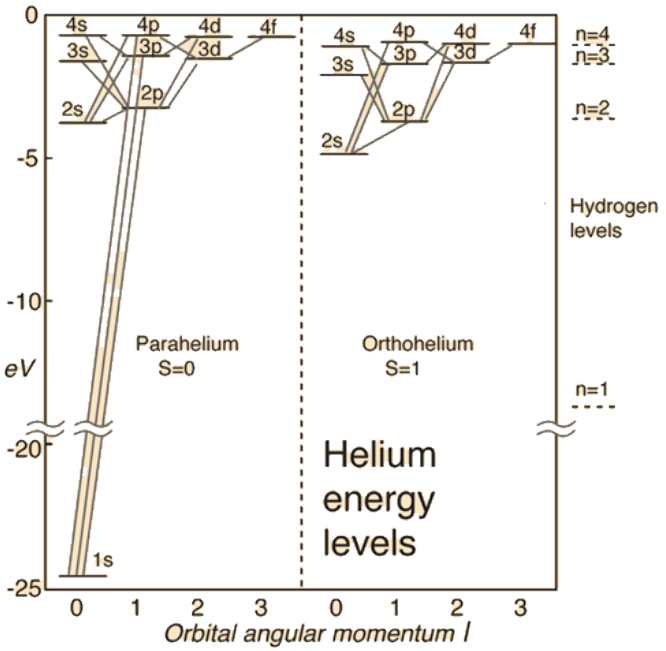

Figure 1: Helium Energy levels in both single at triplet states[4]

2.6 Fabry-Perot Interferometer

Fabry-Perot interferometer as a spectrometer with high resolution is of particular use for fine structure investigation. Fabry-Perot interferometer is made up of two glass (or quartz) plates (fig. 2), which are polished from inside (with precision up to $10^{-2}\lambda$) and set parallel to each other.

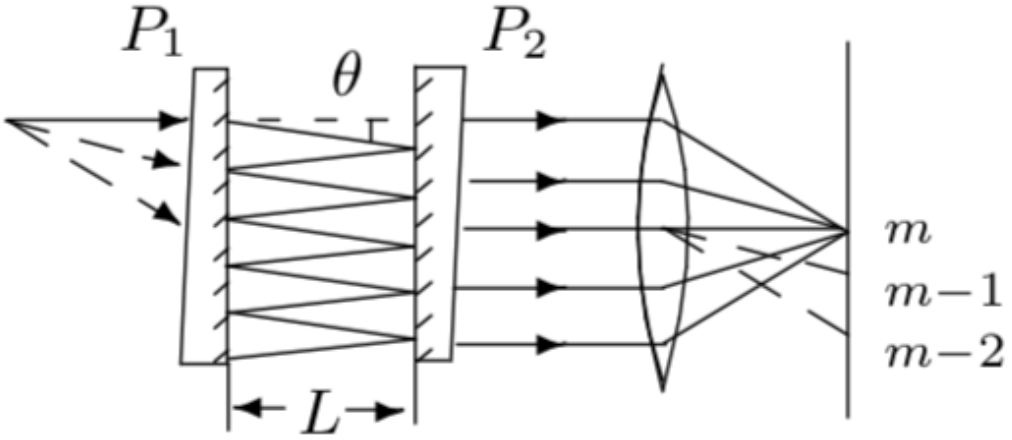

Figure 2: Fabry-Perot interferometer [5].

The Fabry-Perot interferometer can be regarded as a flat-roller air plate with multiple reflections and interference of beams. The interference pattern observed in the focal plane of the lens L consists of concentric rings of equal inclination. For two adjacent beams propagating between the interferometer mirrors at an angle of θ, light travel difference is determined by the ratio:

$$\Delta = 2L\cos\theta = m\lambda \tag{17}$$

where L - distance between mirrors. The diameter of an interference ring can be expressed through the focal lenght of a lens:

$$D = 2f\theta \tag{18}$$

Thus, one can show using the given equation and the one mentioned above:

$$\lambda = \frac{L}{4f^2}\frac{D_j^2 - D_i^2}{j - i} \tag{19}$$

where i, j - numbers of the intereferometer rings and $D_{i,j}$ - diameters of the correspondent rings. For any spectrometer device three main characteristics are considered: dispersion, free spectral range and resolution.

The ratio of the distance dl between the spectral lines in the spectral plane to the wavelength difference $d\lambda$ of these lines is called the linear dispersion D^* of the spectral instrument. For Fabry-Perot it yields:

$$D^* = f\frac{d\Theta}{d\lambda} = \frac{dD}{2d\lambda} = \frac{2f^2}{\lambda D} \tag{20}$$

Another important characteristic is FSR (free spectral range). The maximum wavelength range $\Delta\lambda$ is called the spectral instrument dispersion region, at which the interference bands of neighboring orders have not yet been overlapped. The width of this region is determined by the condition that the ring (m+1)-ordered for the wavelength of λ and the ring m-ordered for the wavelength of $\lambda + \Delta\lambda$:

$$m(\lambda + \Delta\lambda) = (m + 1)\lambda \tag{21}$$

What yields:

$$\Delta\lambda = \frac{\lambda}{m} \approx \frac{\lambda^2}{2L} \tag{22}$$

The order of interference m in Fabry-Perot interferometers is extremely high. Thus, for $\lambda = 5{\cdot}10^{-5}$cm and L=0.5 cm $m \approx 2L/\lambda = 2 * 10^4$, yet $\Delta\lambda = 0.25$A. Thus, the spectral interval, which can be analyzed using the Fabry-Perot interferometer is very small. Therefore, before the Fabry-Perot interferometer, a light filter or other spectral instrument cutting out the spectral bandwidth not exceeding is usually placed. Another important characteristic is its spectral resolution defined as:

$$R = \frac{\lambda}{\delta\lambda} \tag{23}$$

where $\delta\lambda$ is minimum difference in wavelengths allowed by the device in the vicinity of wavelength λ. If we denote the amplitude of the incident light as A_0, and r, t - reflectively and transparency of the interferometer mirrors one can write for the successive beams propagating inside the interferometer:

$$A_0 t, \quad A_0 t r e^{ik\Delta}, \quad A_0 t r^2 e^{i2k\Delta}, \quad A_0 t r^3 e^{i3k\Delta}, \quad \dots \tag{24}$$

What constitute a geometric progression and we can write:

$$A = \frac{A_0 t}{1 - re^{ik\Delta}} \tag{25}$$

and for the intensity:

$$I = AA^* = \frac{I_0 t^2}{1 + r^2 - 2r\cos(k\Delta)} \tag{26}$$

Utilizing the given equation and the Rayleigh criteria we obtain:

$$R \approx \frac{2\pi L\sqrt{r}}{\lambda(1 - r)} \tag{27}$$

for Fabry-Perot spectral resolution.

2.7 CMOS and CCD array

The interference rings could be imaged using the CCD(charge-coupled device) or CMOS(complementary metal-oxide-semiconductors) widely exploited in modern digital cameras. The working principle of these devices is based on the ability to accumulate electric charges proportional to the intensity of light it exposed to. The charges from pixel lines are amplified and read out line by line by shifting the pixel lines. Another light imaging chip CMOS sensor in contrast to CCD has an amplifier for each pixel. In case of a CCD the photoactive region is realized by The components of the basic CCD can be summarized as follows: the photoactive region is realized by the silicon epitaxial layer, the potential wells for accumulating charge - MOS structures (fig.3) and the shifting register - is a combination of such capacitors and gates (fig. 4)

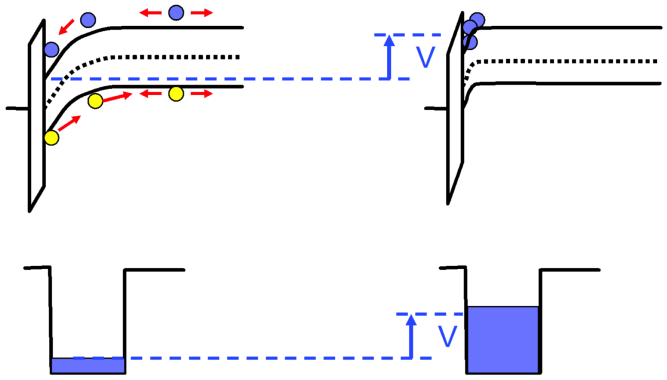

Figure 3: MOS structure as a potential well[6].

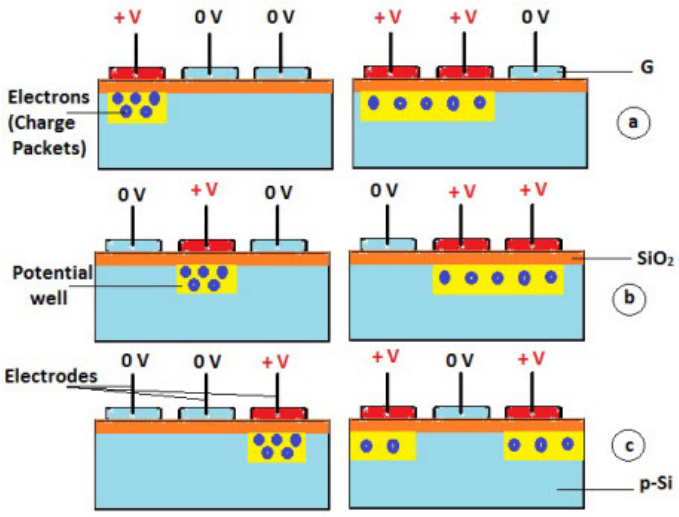

Figure 4: The working principle of a shifting register [7].

3 Apparatus and Method

The apparatus used during the experiment is show schematically in figure 5

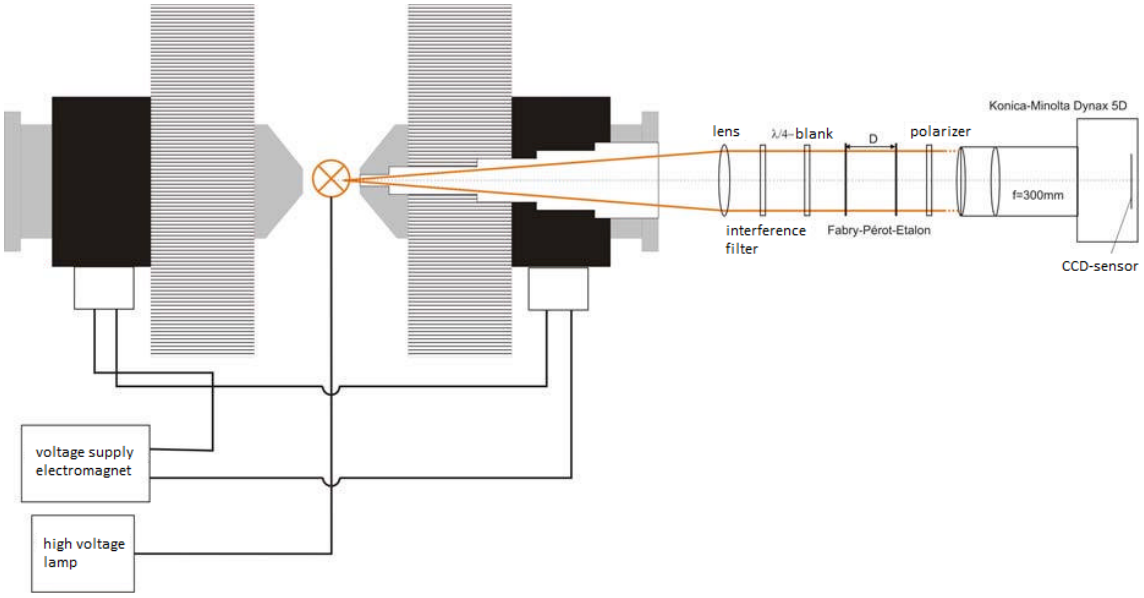

Figure 5: Schematic of the experimental apparatus[1]

The apparatus is made up of a number of components including:

- High Voltage Lamp
- Voltage supply for electromagnet
- lens
- Interference filter
- Quarter wave plate
- Fabry-Perot etalon
- Polarizer
- Konica Minolta Dynax 5D for recording of the output signal.

The goal of the experiment is to observe and analyze the spectrum splitting of Helium $3^3D-2^3P, \lambda = 568.6nm$ under different magnetic field strengths. Before this is done, the apparatus is optimized by first calibrating the magnetic field using the supplied Hall probe, adjusting the optical assembly so that a sharp line is observed and finally, experiment with exposure time, shutter and ISO values to ensure best results. Once this is completed, images are taken of the ring system under varying magnetic field up to 1T. Once this is completed, the experimented is repeated however with the polarisation being changed in 5 degree increments instead.

4 Results and Discussion

4.1 Transverse observation

During the transverse image experiment, images such as that shown in 6 were produced for analysis. These images could be analysed using a python script to extract diameter lengths and thus calculate μ_B.

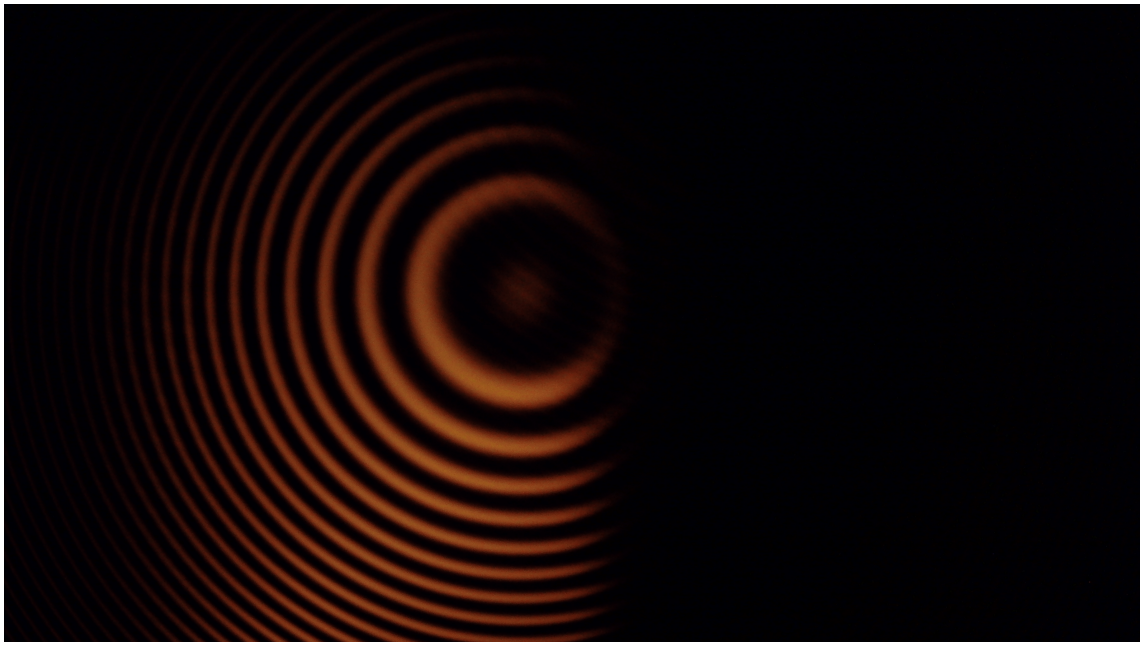

Figure 6: Zeeman effect observed in transverse optical experiment

In order to determine the Bohr magneton, consider the following:

$$\Delta E = \mu_B B \tag{28}$$

$$\lambda = \frac{L}{4f^2}\frac{D_j^2 - D_i^2}{j - i} \tag{29}$$

$$\Delta E = \frac{hc}{\lambda} \tag{30}$$

With this in mind, it is now possible to plot the square of the diameter of each ring and determine the energy between them by examining the difference in their diameter. Upon performing analysis on the results, the following graph for Diameter vs magnetic field is recorded for the Paschen -Back region.

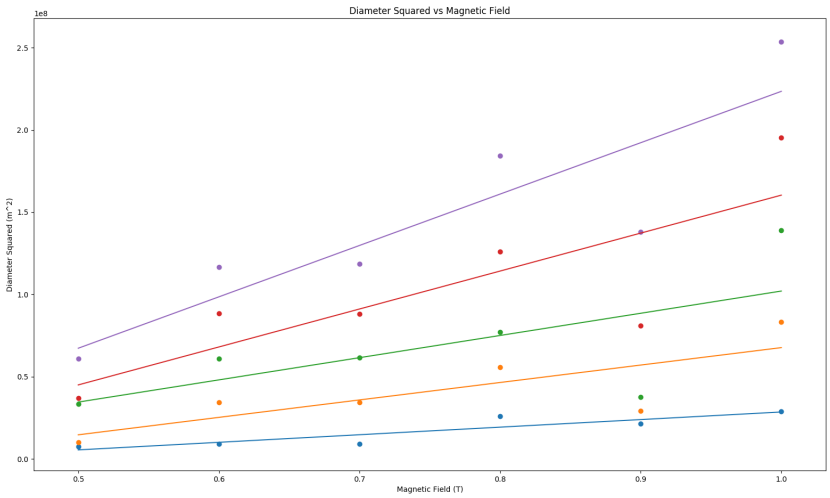

Figure 7: Plot of Diameter squared vs Magnetic Field such that the Bohr magneton can be derived from their differences

The gradients of which allowed for a determination of the Bohr magneton's shown in table 1.

	1-2	2-3	3-4	4-5
μ_B	$1.25 \cdot 10^{-23}$	$2.59 \cdot 10^{-23}$	$7.846 \cdot 10^{-24}$	$9.204 \cdot 10^{-24}$

Table 1: Table outlining Bohr magneton values for various transitions

These values are calculated by considering the energy difference between neighbouring rings and not higher order transitions. During the experiment, complete images were not taken of the rings due to a cover being over the filament. This has lead to difficulties in producing accurate images for analysis, a problem partially resolved by the implementation of a python script to determine radii differences. However, as this program did not accurately locate the centre of the ring system, it was at times inaccurate, especially for the early transitions where a small offset of the centre leads to a large impact measured radii. This error is evident in the gradients of the graphs plotted in figure 7. Each of the gradients should be the equal such that they produce the same value for the Bohr Magneton, this is clearly not the case. Further evidence of this is in the values of μ_B obtained becoming more accurate as the higher energy transitions are considered. Considering this type of error one may state that despite the poor results, error is minimized in the final value which can thus be considered the experimental result, being $9.204 \cdot 10^{-24}$. Comparing this to the Literature value of $9.274 \pm 0.3 \cdot 10^{-24}$[8] we can conclude that the experiment provided at least a single successful measurement of the Bohr Magneton. In future, this error should be rectified so that more data may be used for the analysis. Furthermore, the shielding over the filament should be removed or adjusted such that full images can be taken and more confident result produced.

4.2 Longitudinal observation

The orientation dependence of the Zeeman effect can be understood in classical terms. As is seen from the fig. 8 the $\Delta M_J = 0$ case correspond to a dipole oscillating parallel to the magnetic field, thus no light is emitted along the magnetic field (fig. 10); the light emitted perpendicular to the magnetic field is linearly polarized according to the dipole oscillations. In case of $\Delta M_J = \pm 1$ in contrast to the $\Delta M_J = 0$ the emission along the magnetic field prevails; from classical perspective it can be depicted as a superposition of two circulating around $\vec{B}$ dipoles with 90^o phase difference, thus producing circularly polarized light along the $\vec{B}$ and linearly polarized perpendicular to the field.

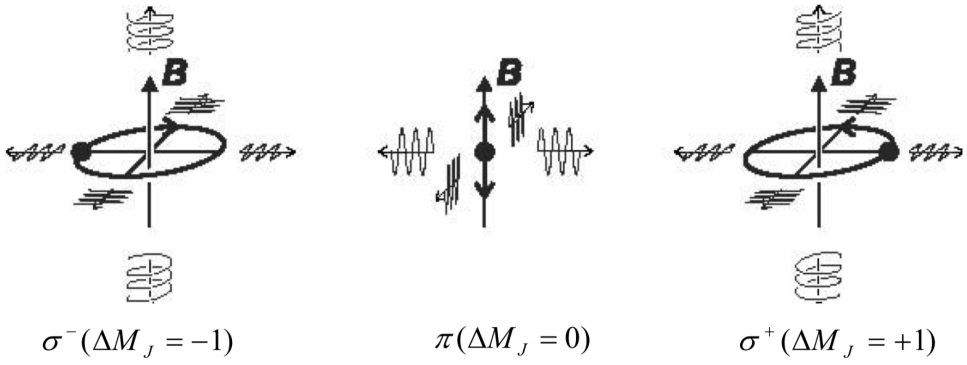

Figure 8: Orientation dependence of the Zeeman effect [9].

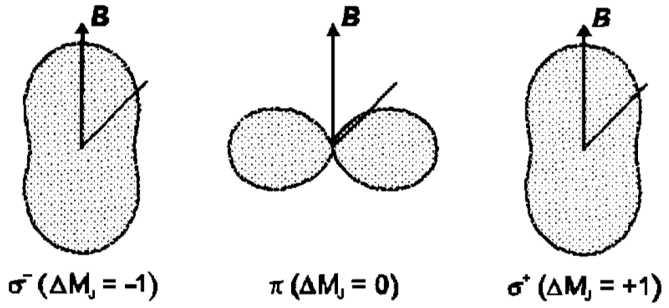

Figure 9: Angular dependence of an electrical dipole emission [9].

The described picture is observed on the experiment. The longitudinal configuration constrains the observed light to only circularly polarized as only circularly polarized light is emitted along the $\vec{B}$. In the given experiment the dependence of the measured interference picture on the polarization is investigated. On the video clip a sequence of rings with polarization varying from 0^o to 90^o with 10^o increment is depicted. The detected light is circularly polarized, as we discussed, thus, we observe σ lines. However, when the $\frac{\lambda}{4}$ is gradually rotated we eventually compensate for the circular polarization and observe linearly polarized π lines.

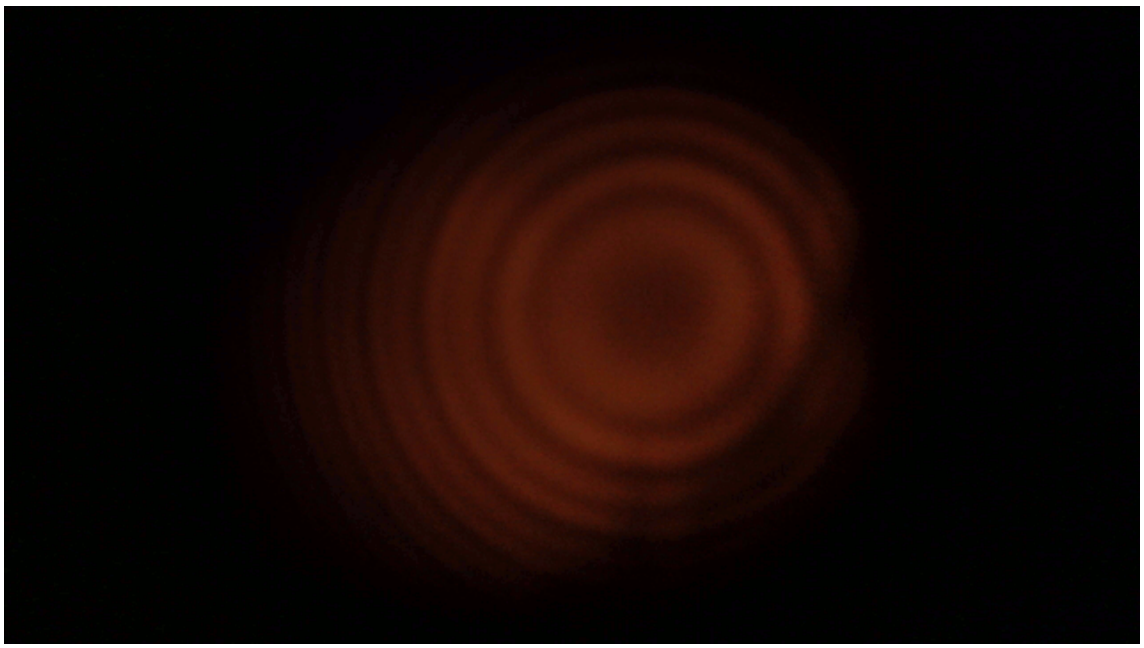

Figure 10: Angular dependence of an electrical dipole emission [9].

5 Conclusion

In this experiment, the Zeeman effect in Helium is probed in both the Zeeman and Paschen-Back regions leading to a determination of the Bohr Magneton of $9.204 \pm 0.3 \cdot 10^{-24}$, very close to the literature value. The largest error came in from the analysis of the lines, ensuring a correct diameter as well as finding the centre of each of the rings. Furthermore, the longitudinal emission has been measured and the clear linearly polarized π lines observed.

References

1. Gompf, B. Zeeman. *Fortgeschrittenen Praktikum* (2012).
2. Haken, H. & Wolf, H. C. *The physics of atoms and quanta* (Springer, 2010).
3. *Optical Pumping* http://instructor.physics.lsa.umich.edu/adv-labs/Optical_Pumping/OpticalPumping2.pdf.
4. Nave, R. *Helium Energy Levels* http://hyperphysics.phy-astr.gsu.edu/hbase/quantum/helium.html.
5. *Fabry-Perot Interferometer* https://mipt.ru/education/chair/physics/S_IV/Opt_man/5.9.pdf.
6. *Charge-Coupled Devices (CCDs)* http://isl.stanford.edu/~abbas/ee392b/lect02.pdf.
7. *Types of Charge-Coupled Devices with their Working Principles* https://www.elprocus.com/know-about-the-working-principle-of-charge-coupled-device/.
8. 2019. https://physics.nist.gov/cuu/Constants/bibliography.html.
9. *Observing the normal Zeeman effect in transverse and longitudinal configuration Spectroscopy with a Fabry-Perot etalon* https://people.stfx.ca/cadams/physics475/labs/zeeman/QueenMaryUnivLondon_Zeeman%20effect.pdf.